The following publication J. Sun, Z. -L. Sun, K. -M. Lam and Z. Zeng, "A Robust Point Set Registration Approach With Multiple Effective Constraints," in IEEE Transactions on Industrial Electronics, vol. 67, no. 12, pp. 10931-10941, Dec. 2020 is available at https://doi.org/10.1109/TIE.2019.2962433.

A Robust Point Set Registration Approach with Multiple Effective Constraints

***Abstract*—How to accurately register point sets still remains a challenging task, due to some unfavorable factors. In this paper, a robust point set registration approach is proposed based on the Gaussian mixture model (GMM) with multiple effective constraints. The Gaussian mixture model is established by wrapping a model point set to a target point set, via a spatial transformation. Instead of a displacement model, the spatial transformation is decomposed as two types of transformations, an affine transformation and a non-affine deformation. For the affine transformation, a constraint term of the parameter vector is applied to improve the robustness and efficiency. In order to enforce the smoothness, the square norm of the kernel Hilbert space is adopted as a coherent constraint for the non-affine deformation. Moreover, the manifold regularization is utilized as a constraint in the proposed model, to capture the spatial geometry of point sets. In addition, the expectation-maximization (EM) algorithm is developed to solve the unknown variables of the proposed model. Compared to the state-of-the-art approaches, the proposed model is more robust to deformation and rotation, due to the use of multiple effective constraints. Experimental results on several widely used data sets demonstrate the effectiveness of the proposed model.**

***Index Terms*—Point set registration, Gaussian mixture model, Expectation-Maximization algorithm.**

I. Introduction

The task of point set registration is to find the correspondence between a model point set and a target point set, and to recover the corresponding mapping transformation. As a critical component, point set registration has been widely applied to many computer vision tasks, including stereo system [1], [2], image retrieval [3], [4], image registration [5], [6], etc.

So far, many effective works have been reported for point pairwise registration. In many earlier studies, to make it more tractable, point set registration was generally simplified in some aspects, such as in terms of the mapping model, outliers, noise, etc. Iterated closest point is one of the most popular algorithms for rigid point set registration, because of its simplicity and low computational complexity [7], [8]. As a simple heuristic method, the correspondence of two point sets was assigned by using the nearest-neighbor relationship in the iterated closest point algorithm. In [9], as an generalization of two-pattern case, an iterative solution was derived based on the expectation-maximization (EM) [10], for global registration of multiple d-dimensional point patterns. For point set registration, the model simplification may make the established model significantly deviate from the true conditions in real-world applications.

In order to obtain more robust solutions, some probabilistic methods have been developed by using the soft assignment of correspondences, which establishes correspondences between all combinations of points, according to probabilities. In [11], a thin-plate spline-based robust point matching algorithm (TPS-RPM) was proposed to solve non-rigid mapping, as well as the correspondences in the presence of noise and outliers. The thin-plate spline was devised as the parameterizations of the non-rigid spatial mapping and the soft assignment for the correspondence, which was estimated by deterministic annealing technique. As deterministic annealing is a heuristics optimization method, the globally optimal solution may not be achieved for TPS-RPM. To address this issue, an asymmetric point matching (APM) algorithm was proposed in [12] by eliminating the transformation variables in the TPS-RPM objective function. Moreover, in order to improve the performance, the parameter vector was weighted by a positive semidefinite matrix and used a robustness constraint.

As an effective model, Gaussian mixture model (GMM) has been widely applied on point set registration. In [13], point set registration was reformulated as a problem of aligning two Gaussian mixtures by minimizing a statistical discrepancy measure. A line segment based automatic image registration method was proposed in [14] using GMM and the EM algorithm. In the image registration method, the probabilistic point registration method is extended for line segments by assuming an equal isotropic covariance and a constant prior of outlier. Moreover, the corresponding line segments may not share the same start points and end points. In [15], an automatic multi-view registration method was reported for multi-view point cloud registration based on the EM algorithm. A robust estimator, named the L_2-minimizing estimator, was employed to build robust sparse and dense correspondences [16]. A particular advantage of [16] is to handling significant scale changes and rotations. In order to remove mismatches from given putative image feature correspondences, an efficient approach, termed as locality preserving matching, was designed by maintaining the local neighborhood structures of potential true matches [17].

For highly cluttered scenes, a rotation invariant non-rigid point set matching algorithm was reported in [18], [19], by matching the graphs that represent two point sets. The graphs were constructed by minimum spanning tree (MST)-induced triangulation and star graph. A point set registration method, spatially constrained context-aware Gaussian fields (SCGF), was proposed in [20], by means of a context-aware representation and a graph Laplacian regularized Gaussian fields. In [21], the local feature, shape context, was used to assign the membership probabilities of the mixture model. Moreover, the transformation between the two point sets was specified in a reproducing kernel Hilbert space, and a sparse approximation was adopted to achieve a fast implementation.

Gradually, the various constraints have been utilized to

improve the performance of GMM. In [22], the points in the target point set were considered as the GMM centroids, and the points in the model point set as the data points generated by the GMM. The coherence constraint, defined as the square norm of reproducing the kernel Hilbert space, was proposed to force the GMM centroids to move coherently as a group, to preserve the topological structure of model point set. In order to identify outliers, point set registration was formulated as a mixture model with a set of latent variables in [23], [24]. Moreover, manifold regularization, a weighted transformation by a graph Laplacian, was imposed on the transformation to capture the intrinsic geometry of a specific shape or object.

Besides pairwise registration, groupwise registration is another category of point set registration [25]. In [26], a groupwise GMM-based registration approach was proposed to create a statistical shape model, via alternately updating the mean shape and registering it to the training shapes. A generative groupwise registration approach, named joint registration of multiple point clouds (JRMPC), was proposed by assuming that multiple point sets are generated from a single GMM [27], [28]. Two types of optimization methods, batch and incremental EM algorithms, were developed to deal with point sets contaminated by noise and outliers.

Nowadays, point set registration still remains a challenging problem, because of the presence of many unfavorable factors in real applications, such as deformation, rotation, etc. In this paper, a robust point set registration approach is proposed based on the Gaussian mixture model (GMM) with multiple effective constraints. Inspired by [11], the transformation is decomposed as a more specific model, i.e. an affine transformation plus a non-affine deformation, instead of a general displacement model [21]–[23]. In order to improve the robustness and efficiency, the affine transformation is given by a linear representation of its parameter vector with a weighted constraint [12]. As a global geometric constraint, a coherent constraint is applied on the non-affine deformation to strengthen the smoothness. Referring to [23], [24], the manifold regularization is considered in the proposed model, to capture the intrinsic geometry of a specific shape or object.

As a major work of this paper, we propose an effective multiple-constraint based GMM model for point set registration. Compared to the state-of-the-art approaches, the proposed model has a more robust performance. Moreover, an expectation-maximization algorithm is developed to solve the unknown variables in the proposed model.

The rest of the paper is organized as follows. The proposed model is introduced in Section II. Experimental results and related discussions are given in Section III. Finally, conclusions are made in Section IV.

II. Methodology

There are two main components in the proposed method: a GMM model with multiple constraints, and the corresponding optimization process using the EM algorithm.

A. GMM Model based on Multiple Constraints

Given a model point set $\mathbf{X} = (\mathbf{x}_1, ..., \mathbf{x}_N)^T \in R^{N\times D}$ with N points in a D-dimensional space, and a target point set $\mathbf{Y} = (\mathbf{y}_1, ..., \mathbf{y}_M)^T \in R^{M\times D}$ with M points in a D-dimensional space, the goal of point set registration is to estimate a transformation $T(\mathbf{X})$ to wrap the model point set to the target point set.

Considering the points in $\mathbf{X}$ as GMM centroids, the points in $\mathbf{Y}$ can be generated by the GMM. Assuming that the outlier distribution is uniform, the mixture model can be formulated as follows,

$$p(\mathbf{y}_m|\boldsymbol{\mu}) = \gamma\frac{1}{N} + \sum_{n=1}^{N}(1-\gamma)P(n)\frac{1}{(2\pi\sigma^2)^{D/2}}e^{-\frac{\|\mathbf{y}_m - T(\mathbf{x}_n)\|^2}{2\sigma^2}}, \tag{1}$$

where σ^2 is the variance of the Gaussian distribution, and γ is the percentage of outliers [22]. From (1), we can see that the GMM centroid locations can be parameterized by a set of unknown parameters, denoted as $\boldsymbol{\mu} = \{T, \sigma^2, \gamma\}$. The parameter set $\boldsymbol{\mu}$ can be estimated by minimizing the following negative log-likelihood function,

$$L(\boldsymbol{\mu}|\mathbf{Y}) = -\sum_{m=1}^{M} lnP(\mathbf{y}_m|\boldsymbol{\mu}). \tag{2}$$

After substituting (1) into (2), the negative log-likelihood function can be rewritten as follows,

$$\begin{aligned} L(\boldsymbol{\mu}|\mathbf{Y}) = &\frac{1}{2\sigma^2}\sum_{m=1}^{M}\sum_{n=1}^{N}P(n|\mathbf{y}_m, \mu^{old})||\mathbf{y}_m - \mathbf{T}(x_n)||^2 \\ &+ \frac{M_p D}{2}ln\sigma^2 - M_p ln(1-\gamma) - (M-M_p)ln\gamma \end{aligned}, \tag{3}$$

where $\boldsymbol{\mu}^{old}$ denotes the current parameter values, and

$$M_p = \sum_{m=1}^{M}\sum_{n=1}^{N}P(n|\mathbf{y}_m, \boldsymbol{\mu}^{old}) \leq M. \tag{4}$$

In terms of the Tikhonov regularization framework, the transformation $T(\mathbf{X})$ can be defined as the initial position plus a displacement function $v(\mathbf{X})$, i.e.,

$$T(\mathbf{X}) = \mathbf{X} + v(\mathbf{X}). \tag{5}$$

In [22], the optimal $v(\mathbf{X})$ was derived as a linear combination of the kernel functions centered at the points $\mathbf{X}$, i.e.,

$$v(\mathbf{X}) = \mathbf{GW}, \tag{6}$$

where $\mathbf{W}$ is a matrix of coefficients, and $\mathbf{G}$ is a kernel matrix with elements g_{ij}, as follows:

$$g_{ij} = e^{-\frac{1}{\varepsilon}||x_i - x_j||^2}, \tag{7}$$

where ε is a tolerated error. In order to enforce the smoothness of v, the square norm of a reproducing kernel Hilbert space is used as a coherent constraint, and denoted as $\phi_1(v)$, as follows:

$$\phi_1(v) = \|v\|_{\mathcal{H}}^2 = tr(\mathbf{W}^T\mathbf{GW}), \tag{8}$$

where $tr(\cdot)$ denotes the trace.

In (5), the displacement function $v(\mathbf{X})$ is a general displacement function with a coherent constraint. Referring to (5) and [11], the spatial transformation $T(\mathbf{X})$ can be decomposed as

two types of transformations, an affine transformation $T_a(\mathbf{X})$ and a non-affine deformation $v(\mathbf{X})$, i.e.,

$$T(\mathbf{X}) = T_a(\mathbf{X}) + v(\mathbf{X}). \tag{9}$$

Compared to (5), (9) is a more specific decomposition. Furthermore, referring to [12], the affine transformation $T_a(\mathbf{X})$ can be given by,

$$T_a(\mathbf{X}) = \mathbf{J}(\mathbf{X})\boldsymbol{\theta}, \tag{10}$$

where $\mathbf{J}(\mathbf{X})$ is the Jacobian matrix, and $\boldsymbol{\theta}$ contains the parameters of scale variation, rotation and translation. In order to improve the robustness and efficiency, $\boldsymbol{\theta}$ is enforced by the following constraint,

$$\phi(\boldsymbol{\theta}) = \boldsymbol{\theta}^T\mathbf{H}\boldsymbol{\theta} - 2{\boldsymbol{\theta}_0}^T\mathbf{H}\boldsymbol{\theta}, \tag{11}$$

where $\mathbf{H}$ is a positive semidefinite matrix whose entries represent the weights assigned to the elements of $\boldsymbol{\theta}$. For a 2D affine transformation of one point $\mathbf{x}_i$, (10) has the following form,

$$T_a(\mathbf{x}_i|\boldsymbol{\theta}) = \begin{bmatrix} \theta_1 & \theta_2 \\ \theta_3 & \theta_4 \end{bmatrix} \begin{bmatrix} x_i^1 \\ x_i^2 \end{bmatrix} + \begin{bmatrix} \theta_5 \\ \theta_6 \end{bmatrix} = \mathbf{J}(\mathbf{x}_i)\boldsymbol{\theta}, \tag{12}$$

where the parameters $\boldsymbol{\theta} = [\theta_1, \cdots, \theta_6]^T$ with $[\theta_1, \cdots, \theta_4]^T$ and $[\theta_5, \theta_6]^T$ being linear transformation and translation parts, respectively. In [12], $\boldsymbol{\theta}$ was set as a constant vector $[1\ 0\ 0\ 1\ 0\ 0]^T$. The constraint (11) provides a flexible trade-off between the linear transformation and the translation.

Considering (6), (9) and (10), in the proposed method, the spatial transformation model $T(\mathbf{X})$ is devised as,

$$T(\mathbf{X}) = \mathbf{J}(\mathbf{X})\boldsymbol{\theta} + \mathbf{GW}, \tag{13}$$

with the constraint (11). Moreover, similar to [22], the coherent constraint (8) is also applied on the non-affine deformation $v(\mathbf{X})$ to enforce the smoothness.

For CPD, the transformation learning focuses on how to utilize the global geometric constraint on the point sets, to obtain a smooth transformation. Referring to [23], [24], the manifold regularization is also considered in the proposed method, to capture the intrinsic geometry of a specific shape or object, i.e.,

$$\phi_2(v) = tr(\mathbf{T}^T\mathbf{AT}). \tag{14}$$

Substitute (13) into (14), $\phi_2(v)$ can be rewritten as,

$$\phi_2(v) = tr((\mathbf{J}\boldsymbol{\theta} + \mathbf{GW})^T\mathbf{A}(\mathbf{J}\boldsymbol{\theta} + \mathbf{GW})), \tag{15}$$

In (15), $\mathbf{A}$ can be given by,

$$\mathbf{A}_{ij} = \mathbf{G}_{ij}^d - \mathbf{G}_{ij}, \tag{16}$$

where $\mathbf{G}^d = diag(\Sigma_{j=1}^M \mathbf{G}_{ij})$, i.e., the diagonal matrix whose i-th entry is the sum of the weights of edges leaving $\mathbf{x}_i$ [23].

Considering (3), (8), (11), and (15), the negative log-likelihood function of the proposed model can be formulated, as follows:

$$\begin{aligned} L(\boldsymbol{\mu}|\mathbf{Y}, \boldsymbol{\theta}) &= \frac{1}{2\sigma^2}\sum_{m=1}^{M}\sum_{n=1}^{N} P(n|\mathbf{y}_m, \mu^{old})||\mathbf{y}_m - \mathbf{T}(\mathbf{x}_n)||^2 \\ &+ \frac{M_pD}{2}ln\sigma^2 - M_pln(1-\gamma) - (M-M_p)ln\gamma \\ &+ \frac{\lambda_1}{2}\phi(\boldsymbol{\theta}) + \frac{\lambda_2}{2}\phi_1(v) + \frac{\lambda_3}{2}\phi_2(v), \end{aligned} \tag{17}$$

where λ_1, λ_2, and λ_3 are the coefficients of the respective regularization terms.

B. The EM algorithm

For the negative log-likelihood function (17), the EM algorithm is adopted to solve the unknown variables $\boldsymbol{\theta}$, γ, σ^2, and $\mathbf{W}$. The optimization process is alternated between two steps: an expectation step (E-step) and a maximization step (M-step).

1) Expectation step

Given the current parameters $\boldsymbol{\mu}^{old}$, the posterior probability p_{mn} can be defined as follows:

$$p_{mn} = P(n|\mathbf{y}_m, \mu^{old}). \tag{18}$$

The posterior probability p_{mn} indicates the degree of the observed data point y_m coinciding with the model point x_n under the current estimated transformation T. In terms of Bayes rule, (18) can be rewritten as follows:

$$\begin{aligned} p_{mn} &= \frac{P(\mathbf{y}_m|n, \boldsymbol{\mu}^{old})P(n|\boldsymbol{\mu}^{old})}{P(\mathbf{y}_m|\boldsymbol{\mu}^{old})} \\ &= \frac{\pi_{mn}e^{-\frac{\|\mathbf{y}_m - \mathbf{T}(\mathbf{x}_n)\|^2}{2\sigma^2}}}{\sum_{k=1}^{N}\pi_{mk}e^{-\frac{\|\mathbf{y}_m - \mathbf{T}(x_k)\|^2}{2\sigma^2}} + \frac{\gamma(2\pi\sigma^2)^{(D/2)}}{(1-\gamma)N}}, \end{aligned} \tag{19}$$

where π_{mn} is the membership probability of the GMM [21]. In the expectation step, each element of the posterior probability matrix $\mathbf{P}$ is computed via (19).

2) Maximization step

After obtaining the posterior probability matrix $\mathbf{P}$, the latent variables are estimated by the gradient descent algorithm. Firstly, the derivative of $L(\boldsymbol{\mu}|\mathbf{Y}, \boldsymbol{\mu}^{old}, \boldsymbol{\theta})$ with respect to $\boldsymbol{\theta}$ can be computed as follows:

$$\begin{aligned} \frac{\partial L}{\partial \boldsymbol{\theta}} &= \frac{1}{\sigma^2}(\mathbf{J}^T\mathbf{J}\boldsymbol{\theta} - \mathbf{J}^T\mathbf{PGW}) + 2\lambda_1(\mathbf{H}\boldsymbol{\theta} - \mathbf{H}^T\boldsymbol{\theta}_0) \\ &+ 2\lambda_3(\mathbf{J}^T\mathbf{AJ} - ((\mathbf{GW})^T\mathbf{AJ})^T). \end{aligned} \tag{20}$$

Let $\frac{\partial L}{\partial \boldsymbol{\theta}}$ be zero, then we can obtain the estimated $\boldsymbol{\theta}$, as follows:

$$\begin{aligned} \boldsymbol{\theta} &= (2\lambda_1\mathbf{H} + 2\lambda_3\mathbf{J}^T\mathbf{AJ} + \frac{1}{\sigma^2}\mathbf{J}^T\mathbf{J})^{-1}(\frac{1}{\sigma^2}\mathbf{J}^T\mathbf{PGW} \\ &+ 2\lambda_1\mathbf{H}^T\boldsymbol{\theta}_0 - 2\lambda_3((\mathbf{GW})^T\mathbf{AJ})^T). \end{aligned} \tag{21}$$

Given $\boldsymbol{\theta}$, the transformation $T(\mathbf{X})$ can be estimated by (13). Substituting $\boldsymbol{\theta}$ and $T(\mathbf{X})$ into (17), we obtain

$$\begin{aligned} L &= \frac{1}{2\sigma^2}\sum_{m=1}^{M}\sum_{n=1}^{N} p_{mn}||\mathbf{y}_m - \mathbf{J}\boldsymbol{\theta} - \mathbf{GW}||^2 \\ &+ \frac{M_pD}{2}ln\sigma^2 - M_pln(1-\gamma) - (M-M_p)ln\gamma \\ &+ \frac{\lambda_1}{2}\phi(\boldsymbol{\theta}) + \frac{\lambda_2}{2}tr(\mathbf{W}^T\mathbf{GW}) \\ &+ \frac{\lambda_3}{2}tr((\mathbf{J}\boldsymbol{\theta} + \mathbf{GW})^T\mathbf{A}(\mathbf{J}\boldsymbol{\theta} + \mathbf{GW})). \end{aligned} \tag{22}$$

Furthermore, we compute the derivatives of L, with respect to γ, σ^2 and $\mathbf{W}$. Then, the derivatives are all set to zero, and the unknown variables can be estimated as follows:

$$\frac{\partial L}{\partial \gamma} = \frac{M_p}{1-\gamma} - \frac{M-M_p}{\gamma}, \tag{23}$$

$$\gamma = 1 - \frac{M_p}{M}, \tag{24}$$

$$\frac{\partial L}{\partial \mathbf{W}} = -\frac{1}{\sigma^2}\mathbf{GP}(\mathbf{Y}-\mathbf{J}\boldsymbol{\theta}) + \lambda_2\mathbf{GW} + \lambda_3\mathbf{GA}(\mathbf{J}\boldsymbol{\theta}+\mathbf{GW}), \tag{25}$$

$$\mathbf{W} = [\mathbf{PG} + \lambda_2\sigma^2 + \lambda_3\mathbf{AG}\sigma^2]^{-1}[\mathbf{PY} - \mathbf{PJ}\boldsymbol{\theta} - \lambda_3\sigma^2\mathbf{AJ}\boldsymbol{\theta}], \tag{26}$$

$$\begin{aligned}\frac{\partial L}{\partial \sigma^2} = &-\frac{1}{2\sigma^4}(tr(\mathbf{Y}^T d(\mathbf{P}^T 1)\mathbf{Y}) - tr((\mathbf{PY})^T\mathbf{T}) \\ &- tr(\mathbf{T}^T d(\mathbf{P}1)\mathbf{T})) + \frac{M_p D}{2\sigma^2},\end{aligned} \tag{27}$$

$$\sigma^2 = \frac{1}{M_p D}(tr(\mathbf{Y}^T d(\mathbf{P}^T 1)\mathbf{Y}) - tr((\mathbf{PY})^T\mathbf{T}) - tr(\mathbf{T}^T d(\mathbf{P}1)\mathbf{T})). \tag{28}$$

The optimization process of the proposed model is summarized in Algorithm 1.

Algorithm 1 The MC-RPM Algorithm.

1: Input: Model point set $\mathbf{X}$, target point set $\mathbf{Y}$, the initial parameters λ_1, λ_2, λ_3, ϵ;
2: Output: the transformation $T(\mathbf{X})$;
3: Initialize: $\mathbf{W} = \mathbf{0}$, $\sigma^2 = \frac{1}{DMN}\sum_{m,n=1}^{M,N}||\mathbf{y}_m - \mathbf{x}_n||^2$;
4: Compute $\mathbf{G}$ and $\mathbf{A}$ using (7) and (16), respectively;
5: Compute $T(\mathbf{X})$ using (13);
6: **repeat**
7: E-step:
8: Update the matrix $\mathbf{P}$ by (19);
9: M-step:
10: Update $\boldsymbol{\theta}$ with (21);
Compute $T(\mathbf{X})$ with (13);
Update γ, $\mathbf{W}$ and σ^2 by (24), (26) and (28), respectively;
11: **until** convergence;
12: Compute the final $T(\mathbf{X})$ with (13).

C. Similarity and difference of the related methods

The proposed method, denoted as MC, is related to three point set registration algorithms, i.e. coherent point drift (CPD) [22], manifold regularization method (MR) [23], [24], and non-rigid point set registration by preserving global and local structures (PR-GLS) [21]. Table I tabulates the similarity and difference of four related methods.

The proposed method and three related methods are all based on the GMM. In CPD, the parameter γ is set as a constant to simplify the optimization. Except for CPD, the parameter γ is adaptively optimized for other three methods in the model optimization process.

The transformation $T(\mathbf{X})$ is decomposed as the initial position plus a displacement function $v(\mathbf{X})$, i.e., (5), for CPD, MR, and PR-GLS. Different from these three methods, $T(\mathbf{X})$ is decomposed as an affine transformation and a non-affine deformation, i.e. (13), for MC.

For the four methods, different constraints are utilized in the respective models. Considering the function and definition, Table II shows a brief summary for three types of constraints. The coherent constraint, i.e. (8), is used in all these four methods. The manifold regularization term is adopted in both MR and MC. Nevertheless, different from MR, the transformation (13) is considered in the manifold regularization term of MC, instead of (5). In addition, different from other three methods, the robustness constraint, i.e. (11), is applied on the parameter vector $\boldsymbol{\theta}$ for MC. Except for CPD, the local feature, shape context, is utilized to compute the correspondence $\mathbf{P}$ for other three methods.

III. Experimental results

A. Experimental data and set-up

The performance of the proposed method is evaluated on four types of data, including the synthetic data from two classical shapes [11], three sets of data with arbitrary shapes [11], three sequences used for non-rigid structure from motion (NSFM) [29], and four 3D sequences [29], [30].

To evaluate the performance of our proposed method, we compare it to five state-of-the-art algorithms for point set registration, including APM [12], CPD [22], MR [23], [24], SCGF [20], and PR-GLS [21]. All simulations were conducted in the Matlab environment, running on an ordinary personal computer with dual 3.2-GHz CPUs and 4-GB memory.

In order to measure the estimation performance, the average mean-squared error ϵ of the 2D coordinates between the estimated 2D shape ($T(\mathbf{X})$) and the true 2D shape ($\mathbf{Y}$) is used as the performance index, i.e.,

$$\epsilon = \frac{1}{M}\|T(\mathbf{X}) - \mathbf{Y}\|_F^2. \tag{29}$$

A smaller ϵ means that the estimation of an algorithm is more accurate.

For the proposed method, one problem is how to determine the weighting coefficients λ_1, λ_2, and λ_3 in (17). For other methods, there are usually several weighting coefficients to be optimized. As no training is required for point set registration, traditional parameter-selection methods, such as cross validation, cannot be used to choose the optimal parameters. Generally, most point set registration algorithms attempt to find the optimal parameter values by trial and error. In the experiments, the approximately optimal values for the weighting coefficients are determined by the grid search for all the methods.

B. Experimental comparisons

1) Experimental comparisons on the synthetic data

A series of synthetic data is designed to compare the robustness of the various point registration algorithms. Two classic shapes, a fish and a Chinese character *Fu*, are used as the template shapes in the experiments.

As in [19], the Gaussian radial basis function is used to generate non-rigid deformations with coefficients sampled from a Gaussian distribution. The deformation parameter β is varied from 0.02 to 0.2 to control the deformation extent [12]. Figure 1 shows the template point sets (left column), and some examples of target point sets with different deformation extents. For each deformation parameter β, non-rigid deformation is enforced on the model shape to generate 10 sets of target points via varying the coefficients of random sampling.

TABLE I
The similarity and difference of four related methods.

Method	Gaussian mixture model (GMM)	Transformation function $T(\mathbf{X})$	Constraints
CPD	(a) GMM (1) (b) γ is set as a constant	the initial position plus a displacement function, i.e. (5)	(a) coherent constraint (8); (b) compute the correspondence matrix $\mathbf{P}$ via the Bayes rule.
PR-GLS	(a) GMM (1) (b) γ is optimized	the initial position plus a displacement function, i.e. (5)	(a) coherent constraint (8); (b) compute the membership probabilities π_{mn} via the local feature-shape context; compute the correspondence matrix $\mathbf{P}$ via the Bayes rule.
MR	(a) GMM (1) (b) γ is optimized	the initial position plus a displacement function, i.e. (5)	(a) coherent constraint (8); (b) manifold regularization (14); (c) search for the initial correspondences via the local feature-shape context; compute the correspondence matrix $\mathbf{P}$ via the Bayes rule.
MC	(a) GMM (1) (b) γ is optimized	an affine transformation and a non-affine deformation, i.e. (13)	(a) coherent constraint (8); (b) manifold regularization (15); (c) robustness constraint $\phi(\theta)$, i.e. (11); (d) compute the membership probabilities π_{mn} via the local feature-shape context; compute the correspondence matrix $\mathbf{P}$ via the Bayes rule.

TABLE II
A summary of three types of constraints.

Constraint	Function	Definition
coherent constraint	enforce the smoothness of $\upsilon(\mathbf{X})$ by forcing the GMM centroids to move coherently as a group, to preserve the topological structure of the model point set.	Eq. (8), the square norm of a reproducing kernel Hilbert space for the displacement function $\upsilon(\mathbf{X})$.
manifold regularization	capture the intrinsic geometry of a specific shape or object.	Eq. (14), weight the transformation by a graph Laplacian $\mathbf{A}$.
robustness constraint	improve the robustness and efficiency.	Eq. (11), weight the parameter vector. $\boldsymbol{\theta}$ by a positive semidefinite matrix $\mathbf{H}$.

TABLE III
The mean and variance ($\mu \pm \sigma^2$) of the registration errors of six methods when the deformation parameter β is set as different values for the fish point sets.

β	CPD	PR-GLS	APM	SCGF	MR	MC
0.02	4.4593e-06±1.2232e-11	8.2121e-06±2.9820e-11	0.0076±2.1482e-05	0.0019±3.8461e-06	2.3675e-05±3.4453e-11	5.8852e-06±1.6340e-11
0.04	7.9365e-06±4.0493e-11	1.0178e-05±5.6181e-11	0.0151±8.5928e-05	0.0022±8.0069e-06	1.1240e-04±2.0845e-08	8.1177e-06±4.2916e-11
0.06	6.5879e-06±4.7784e-11	6.9886e-06±8.3214e-11	0.0230±2.0230e-04	0.0033±5.6579e-06	3.5780e-04±2.3423e-07	9.4294e-06±3.7709e-11
0.08	1.1541e-05±6.4640e-11	1.1916e-05±5.3233e-11	0.0324±3.8236e-04	0.0030±3.9864e-06	0.0013±3.0413e-06	9.4754e-06±2.1879e-11
0.10	0.0013±5.9017e-06	8.4846e-06±2.4345e-11	0.0414±6.7955e-04	0.0058±4.5173e-05	0.0035±2.6987e-05	9.1648e-06±1.0531e-11
0.12	0.0023±1.0136e-05	2.1257e-05±6.1211e-10	0.0521±0.0010	0.0069±2.1458e-05	0.0078±1.0960e-04	1.2598e-05±4.4563e-11
0.14	0.0054±5.4866e-05	1.6715e-05±7.4998e-11	0.0636±0.0016	0.0127±0.0001	0.0122±1.3745e-04	1.2185e-05±5.4957e-11
0.16	0.0185±7.9725e-04	3.0822e-05±3.5776e-10	0.0790±0.0017	0.0195±0.0002	0.0149±1.4594e-04	1.4793e-05±6.6163e-11
0.18	0.0515±0.0020	0.0125±0.0014	0.0959±0.0023	0.0235±0.0003	0.0184±2.3816e-04	1.6655e-05±7.1878e-11
0.20	0.0566±0.0034	0.0236±0.0024	0.1136±0.0032	0.0327±0.0003	0.0230±2.6955e-04	1.5992e-05±6.0009e-11

TABLE IV
The mean and variance ($\mu \pm \sigma^2$) of the registration errors of six methods when the deformation parameter β is set as different values for the Chinese character *Fu*.

β	CPD	PR-GLS	APM	SCGF	MR	MC
0.02	7.1199e-06±2.8405e-11	1.0546e-05±1.0040e-10	0.0115±2.1482e-05	0.0021±6.0784e-06	0.0076±2.1482e-05	5.4227e-06±2.3634e-11
0.04	1.0047e-05±3.4787e-11	1.8691e-04±8.9630e-10	0.0232±2.1654e-04	0.0059±3.2488e-05	0.0151±8.5928e-05	7.2902e-06±2.1768e-11
0.06	8.4086e-06±8.9433e-11	6.7742e-04±4.3834e-06	0.0365±5.7457e-04	0.0035±2.2845e-06	0.0230±2.0230e-04	1.0991e-05±6.1716e-11
0.08	0.0034±2.5425e-05	0.0017±4.3631e-04	0.0609±0.0024	0.0100±8.674e-05	0.0324±3.8236e-04	1.2640e-05±4.1978e-11
0.10	0.0367±0.0050	0.0164±2.4345e-11	0.0776±0.0038	0.0107±0.0001	0.0414±6.7955e-04	1.6911e-05±1.0414e-11
0.12	0.0764±0.0159	0.0339±0.0019	0.1001±0.0044	0.0195±0.0005	0.0271±5.6589e-04	2.1578e-05±9.3018e-11
0.14	0.0959±0.0238	0.0571±0.0044	0.1293±0.0081	0.0208±0.0002	0.0382±5.3476e-04	0.0028±7.8077e-05
0.16	0.1400±0.0277	0.0893±0.0079	0.1566±0.0110	0.0253±0.0006	0.0496±6.9655e-04	0.0052±2.6486e-04
0.18	0.1837±0.0315	0.1123±0.0104	0.1769±0.0131	0.0296±0.0003	0.0474±5.1241e-04	0.0079±2.8597e-04
0.20	0.2219±0.0456	0.1611±0.0156	0.2174±0.0133	0.0504±0.0014	0.0565±0.0011	0.0168±0.0010

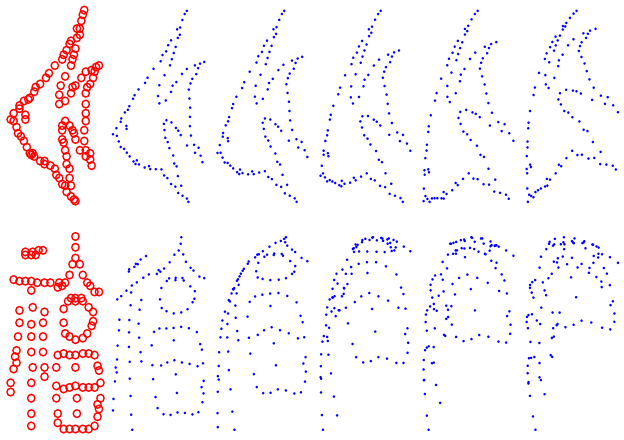

Fig. 1. The template point sets (left column), and some examples of target point sets with different deformation extents.

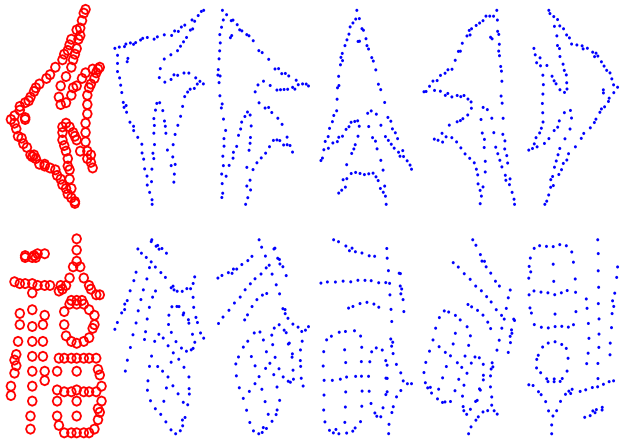

Fig. 2. The template point set (left column), and some examples of target point sets with different rotation angles.

After ten trials, we compute the mean and variance ($\mu \pm \sigma^2$) of the registration errors ϵ of ten sets of data.

Tables III and IV show the mean and variance ($\mu \pm \sigma^2$) of the registration errors of the six methods, when the deformation parameter β is set at different values. In order to easily compare the performance of different algorithms, the best result and the second-best result are highlighted in red and blue, respectively. It can be seen from Tables III and IV that, when β is less than 0.08, the registration errors of CPD and MC are smaller than that of the other methods. Moreover, the registration errors of PR-GLS, MR, and MC are smaller than that of the other methods, when β is larger than or equal to 0.08. This indicates that, MC can achieve a better registration performance for these two shapes with different deformation extents, especially for larger deformation.

In order to test the robustness of the various methods against rotation, the template point set is rotated at different angles, to generate the target point sets. Figure 2 shows the template point sets (left column), and some examples of target point sets with different rotation angles.

Tables V and VI show the mean and variance ($\mu \pm \sigma^2$) of the registration errors of the six methods, when the rotation angle δ is set at different values. Generally, the registration errors of MC are smaller than that of the other methods for most sequences. Therefore, the performance of MC is better than that of the other algorithms for these two shapes, rotated by different angles.

2) Experimental comparisons on three irregular shapes

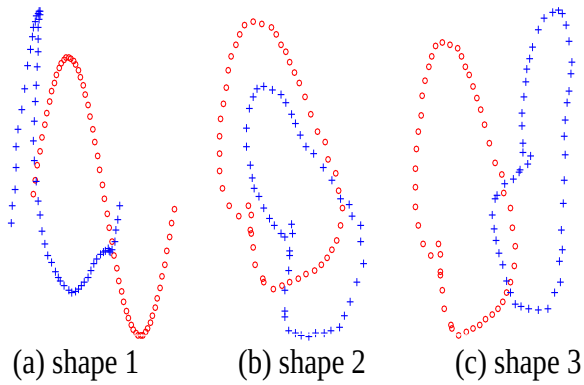

Fig. 3. Three pairs of template point sets (red) and target point sets (blue) with irregular shapes.

Figure 3 shows three pairs of template point sets (red) and target point sets (blue) with irregular shapes. Table VII tabulates the registration errors of the six methods for three irregular shapes. The registration errors of MR and MC

TABLE V
The mean and variance ($\mu \pm \sigma^2$) of the registration errors of six methods when the rotation angle δ is set as different values for the fish point sets.

δ	CPD	PR-GLS	APM	SCGF	MR	MC
30	1.9130e-05±3.6067e-07	1.2511e-05±6.2696e-11	0.0076±2.1482e-05	0.0018±1.3812e-06	2.4335e-04±1.7959e-08	1.0914e-05±6.3978e-11
60	0.0792±0.0166	0.0344±0.0022	0.0076±2.1482e-05	0.0031±8.5259e-07	0.0364±9.7027e-06	1.0316e-05±1.5987e-11
90	0.3441±3.9156e-04	0.2959±4.9891e-04	0.0076±2.1482e-05	0.0027±6.3074e-07	0.0372±1.9666e-05	1.0305e-05±3.1017e-11
120	0.3528±3.9156e-04	0.3727±8.1139e-04	0.0076±2.1482e-05	0.0072±6.5098e-05	0.0433±1.3273e-05	1.3148e-05±2.1707e-11
180	0.4045±5.3455e-04	0.4228±6.0702e-04	0.0076±2.1482e-05	0.4012±0.0164	0.0449±5.9404e-06	1.3588e-05±3.5255e-11

TABLE VI
The mean and variance ($\mu \pm \sigma^2$) of the registration errors of six methods when the rotation angle δ is set as different values for the Chinese character *Fu*.

δ	CPD	PR-GLS	APM	SCGF	MR	MC
30	0.4045±5.3455e-04	6.5265e-06±1.2492e-11	0.0115±5.1650e-05	0.0024±4.8074e-07	0.0195±6.1853e-04	1.1526e-05±1.2787e-11
60	0.3399±0.0020	0.0773±0.0100	0.0115±5.1650e-05	0.0053±3.1456e-06	0.0436±1.2348e-05	1.2391e-05±4.2679e-11
90	0.3718±3.7017e-04	0.3463±5.9352e-04	0.0115±5.1650e-05	0.0117±5.8066e-05	0.0451±5.2152e-06	1.3371e-05±1.3654e-11
120	0.4526±5.6670e-04	0.3880±0.0011	0.0115±5.1650e-05	0.0089±0.0002	0.0456±6.1066e-06	1.4607e-05±3.5719e-11
180	0.5510±8.1384e-04	0.5380±8.2390e-04	0.0115±5.1650e-05	0.5612±0.0007	0.0473±1.9432e-05	0.3814±0.0415

TABLE VII
The registration errors of the six methods for three irregular shapes.

Shape	CPD	PR-GLS	APM	SCGF	MR	MC
1	0.0252	0.0109	0.1020	0.0224	0.0095	0.0099
2	0.0181	0.0065	0.0452	0.0198	0.0042	0.0048
3	0.1670	0.0111	0.1817	0.0145	0.0334	0.0049

are obviously smaller than that of the other four methods. Compared to MR, the registration errors of MC are slightly larger for shapes 1 and 2, but obviously smaller for shape 3.

3) Experimental comparisons on the 2D sequences for NSFM

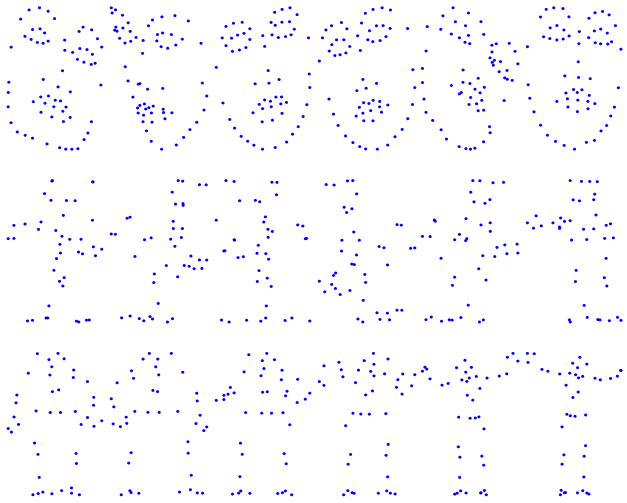

Fig. 4. Some frames of three image sequences used for NSFM.

We also conducted the experiments on three motion sequences: FRGC, pickup and stretch, which are used for NSFM. Figure 4 shows some frames of the three image sequences. In these sequences, the relative camera motions include rotation, deformation and translation. Thus, a comprehensive performance of the various algorithms can be evaluated based on these sequences.

As point set registration is performed between two frames, ten frame pairs are extracted from each of the sequences. Figure 5 (a)-(c) shows the registration errors of six methods for the sequences FRGC, pickup and stretch, respectively. Moreover, Table VIII tabulates the corresponding mean and variance ($\mu \pm \sigma^2$) of the registration errors. We can see from Fig. 5 and Table VIII that, the registration errors of SCGF, MR, and MC are obviously smaller than that of the other three methods. Compared to SCGF and MR, the registration errors of MC are smaller for most frame pairs.

4) Experimental comparisons on 3D data

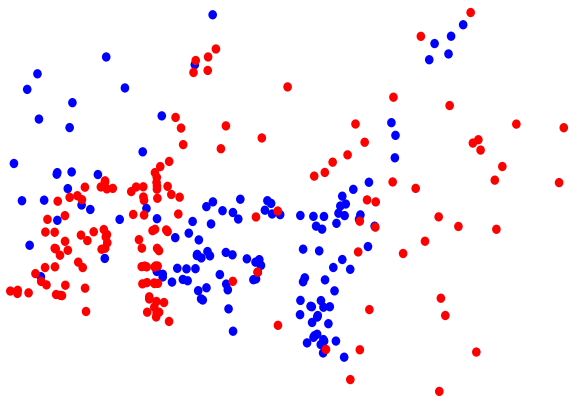

Fig. 6. The 2D scattered points of the template point set (blue color) and the target point set (red color) for 3D horse sequence.

Besides 2D data, we also performed the experimental comparisons on four 3D sequences, i.e. FRGC, pickup, stretch, and horse (Fig. 6). Different from other three 3D sequences, there are five frame pairs in the sequence horse. Figure 7 (a)-(d) shows the registration errors of six methods for four

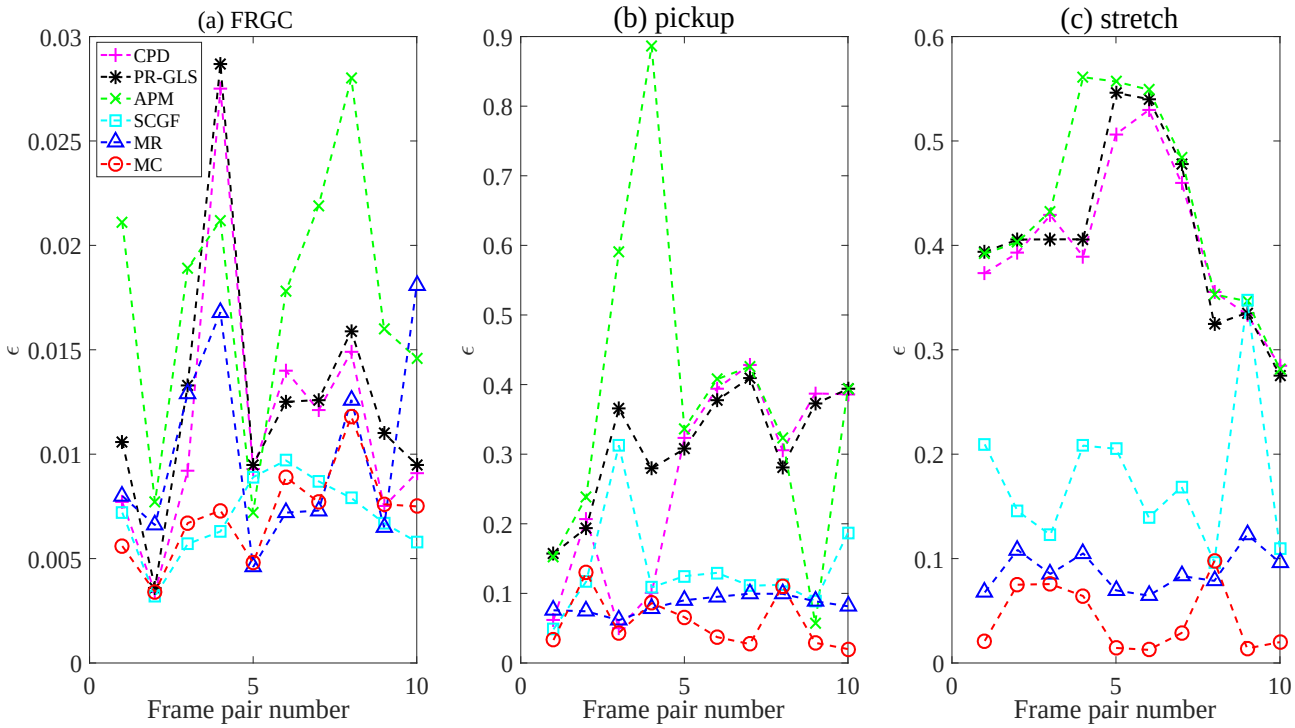

Fig. 5. The registration errors of six methods for three sequences used for NSFM.

TABLE VIII
The mean and variance ($\mu \pm \sigma^2$) of the registration errors of six methods for three sequences used for NSFM.

Sequence	CPD	PR-GLS	APM	SCGF	MR	MC
FRGC	0.0115±4.2900e-05	0.0127±4.1915e-05	0.0174±4.1229e-05	0.0070±3.6432e-06	0.0101±2.2120e-05	0.0071±5.2801e-06
pickup	0.2643±0.0218	0.3814±0.0539	0.3814±0.0539	0.1340±0.0051	0.0842±1.4986e-04	0.0582±0.0015
stretch	0.4054±0.0059	0.4110±0.0079	0.4360±0.0097	0.1834±0.0049	0.0881±3.7955e-04	0.0478±0.0011

TABLE IX
The mean and variance deviation ($\mu \pm \sigma^2$) of the registration errors of six methods for four 3D sequences.

sequence	CPD	PR-GLS	APM	SCGF	MR	MC
FRGC	0.0302±0.0023	0.0315±9.5642e-04	0.0616±0.0048	0.0650±0.0014	0.0131±3.4739e-05	0.0103±1.9094e-06
pickup	0.5008±0.0077	0.5516±0.0018	0.0784±0.0027	0.5926±0.0246	0.1947±0.0021	0.0613±0.0026
stretch	0.4977±0.0090	0.4828±0.0056	0.1074±0.0060	0.5557±0.0065	0.1280±0.0011	0.0614±0.0012
horse	1.0326±0.0052	0.6472±0.0160	0.6284±0.0058	0.9801±0.0148	0.4581±0.0308z	0.3721±0.0064

3D sequences, respectively. Moreover, Table IX tabulates the corresponding mean and variance ($\mu \pm \sigma^2$) of the registration errors. We can see from Fig. 7 and Table IX that, the registration errors of APM, MR, and MC are generally smaller than that of the other three methods. Compared to APM and MR, the registration errors of MC are smaller for most frame pairs.

C. Related discussions

1) The effectiveness of three types of constraints

In order to investigate the effectiveness of three types of constraints, i.e. $\phi_1(v)$, $\phi(\boldsymbol{\theta})$, and $\phi_2(v)$, in the proposed model (17), we conducted the experiments to evaluate the performance of our model, when the different constraint terms are added into (17).

Taking the synthetic data from Fish and Fu, for example, Table X shows the registration errors when deformation and rotation are applied to the model shapes. The performance, using $\phi_1(v)$ only in our proposed model on the deformed and rotated shapes, is first measured. For the synthetic data with rotation, the registration errors are obviously decreased when the constraint term $\phi_2(v)$ is added to capture the spatial geometry of the target point set. When $\phi(\boldsymbol{\theta})$ is combined with $\phi_1(v)$, the registration errors are significantly lower than that of using the single constraint $\phi_1(v)$. Most of the registration errors based on MC are mostly lower than that of using one constraint term or two constraint terms. Therefore, the constraint terms in (17) are all effective for point set register. Moreover, a comprehensive performance can be achieved for the proposed model.

As an example, Table XI shows the registration errors when

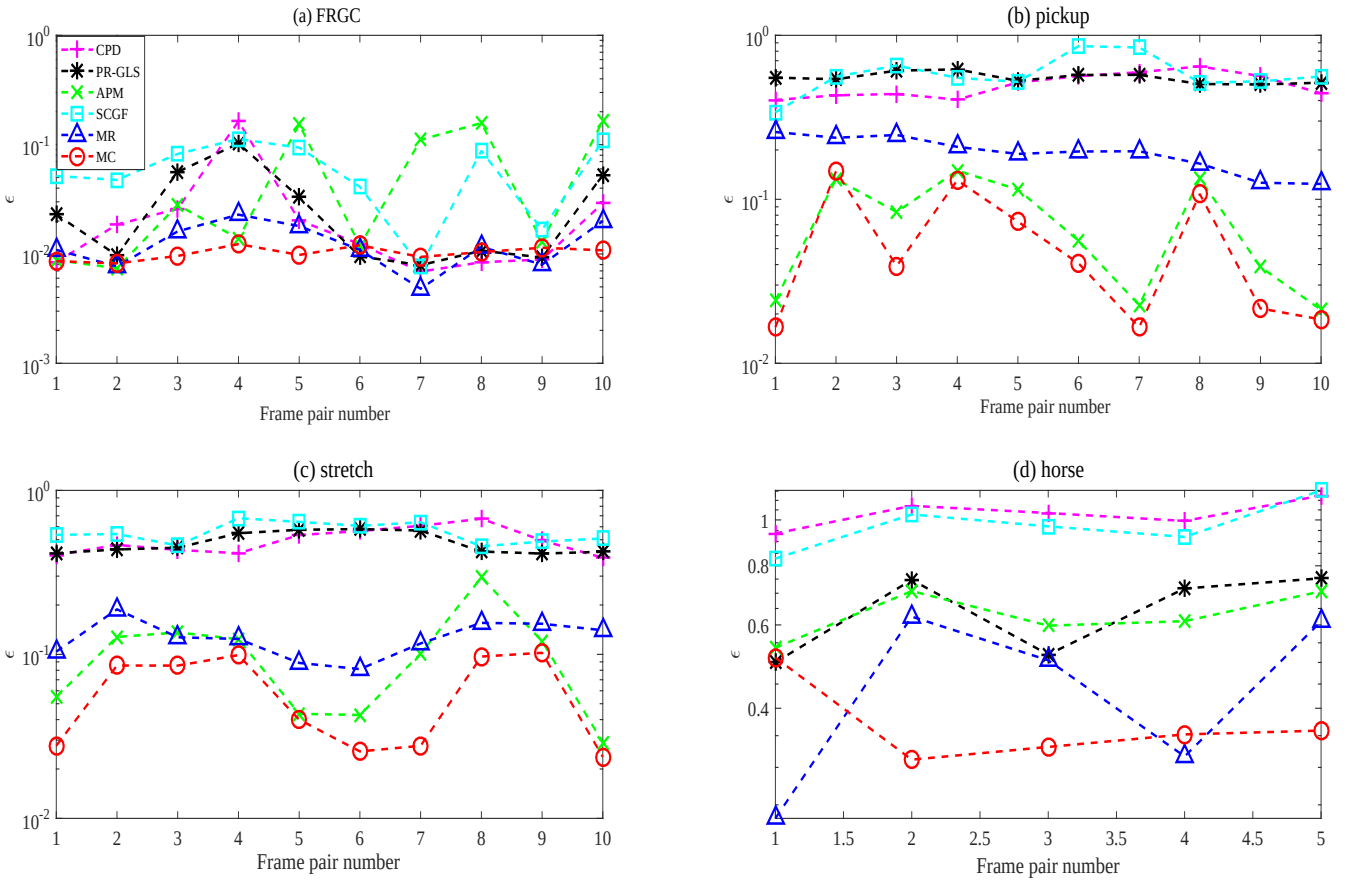

Fig. 7. The registration errors of six methods for four 3D sequences.

TABLE X
The registration errors when different constraint terms are adopted in the proposed model for the synthetic data form Fish and Fu with deformation and rotation.

Data	$\phi_1(v)$	$\phi_1(v)+\phi(\boldsymbol{\theta})$	$\phi_1(v)+\phi_2(v)$	MC
Fish-deformation	0.0236±0.0024	2.6121e-05±6.5053e-10	0.0325±0.0025	1.5992e-05±6.0009e-11
Fu-deformation	0.1611±0.0156	0.0208±0.0012	0.0916±0.0166	0.0168±0.0010
Fish-rotation	0.4228±6.0702e-04	0.3168±0.0186	0.0024±2.6121e-05	1.3588e-05±3.5255e-11
Fu-rotation	0.5380±8.2390e-04	0.5956±0.0011	0.0287±0.0082	0.3814±0.0415

TABLE XI
The registration errors when different constraint terms are adopted in the proposed model for three sequences used for NSFM.

Sequence	$\phi_1(v)$	$\phi_1(v)+\phi(\boldsymbol{\theta})$	$\phi_1(v)+\phi_2(v)$	MC
FRGC	0.0106	0.0057	0.0056	0.0056
pick-up	0.1568	0.0719	0.0328	0.0330
stretch	0.3937	0.0212	0.0226	0.0212

the different constraints are adopted in the proposed model with one frame pair for each of the three sequences used for NSFM. The registration errors of MC are mostly lower than that of using one constraint term or two constraints.

2) Analysis of computational complexity

Referring to [16], the computational complexity is roughly

TABLE XII
The costs of updating the objective function and the unknown parameters for the proposed method.

$L(\boldsymbol{\mu}\|\mathbf{Y},\boldsymbol{\theta})$ Eq. (17)	$\mathbf{W}$ Eq. (26)	γ Eq. (24)	$\boldsymbol{\theta}$ Eq. (21)	σ^2 Eq. (28)
$o(N^2M+N^3)$	$o(N^3)$	$o(N^2M)$	$o(N^3)$	$o(N^2+MN)$

TABLE XIII
The run times (RT, sec.) of different methods for one synthetic data of fish.

method	CPD	PR-GLS	APM	SCGF	MR	MC
RT	0.7607	0.4149	1.1156	107.8571	0.8084	0.5338

analyzed for four related methods, i.e. CPD, PR-GLS, MR, and the proposed method, by considering the costs of updating the objective function and the unknown parameters. For these four methods, the unknown parameters are all solved via the EM algorithm. As the dimension D (2 or 3) is far less than M or N, for simplicity, the effect of D can be neglected in the computational complexity analysis.

For the proposed method, Table XII tabulates the costs of updating the objective function and the unknown parameters. In total, the complexity of the proposed method can be expressed as $o(N^2M + N^3)$. Similarity, the complexities of CPD, PR-GLS, and MR are $o(M^3 + NM^2)$, $o(N^2M + N^3)$, and $o(M^2N+M^3)$, respectively. In general, the computational complexities of four methods are close to each other.

Moreover, take one synthetic data of fish for example, Table XIII shows the run times of different methods. Except for SCGF, the run times are close to each other for five methods.

IV. Conclusions

In this paper, a robust point set registration approach is proposed based on the Gaussian mixture model by utilizing three constraints, namely, the coherent constraint, the robustness constraint, and the manifold regularization term. When the transformation is decomposed as an affine transformation and a non-affine deformation, the registration accuracies can be improved by combining the coherent constraint with the robustness constraint or the manifold regularization term. Generally, the best performance can be achieved for most sequences by combining three constraints simultaneously. Although more constraints are utilized, the computational complexity of the proposed method is close to several related methods, by considering the costs of updating the objective function and the unknown parameters. Experimental results on some widely used data sets demonstrated that, compared to state-of-the-art approaches, a better comprehensive performance can be achieved by the proposed model.

References

[1] S. Schraml, A. N. Belbachir, and H. Bischof, "An event-driven stereo system for real-time 3-D 360 degrees panoramic vision," *IEEE Transactions on Industrial Electronics*, vol. 63, no. 1, pp. 418-428, 2015.

[2] Y. Liu, R. Xiong, Y. Wang, H. Hang, X. Liu, and G. Zhang, "Stereo visual-inertial odometry with multiple kalman filters ensemble," *IEEE Transactions on Industrial Electronics*, vol. 63, no. 10, pp. 6205-6216, 2017.

[3] Y. Gao, M. Wang, R. Ji, and Q. Dai, "3-D object retrieval with hausdorff distance learning," *IEEE Transactions on Industrial Electronics*, vol. 61, no. 4, pp. 2088-2098, 2014.

[4] Y. Motai and A. Kosaka, "Hand-eye calibration applied to viewpoint selection for robotic vision," *IEEE Transactions on Industrial Electronics*, vol. 55, no. 10, pp. 3731-3741, 2008.

[5] B. Jia, J. Chen, and K. Zhang, "Drivable road reconstruction for intelligent vehicles based on two-view geometry," *IEEE Transactions on Industrial Electronics*, vol. 64, no. 5, pp. 3696-3706, 2017.

[6] X. Liu, Y. Ai, B. Tian, and D. Cao, "Robust and fast registration of infrared and visible images for electro-optical pod," *IEEE Transactions on Industrial Electronics*, vol. 66, no. 2, pp. 1335-1344, 2019.

[7] Z. Zhang, "Iterative point matching for registration of free-form curves and surfaces," *International Journal of Computer Vision*, vol. 13, no. 2, pp. 119-152, 1994.

[8] P. J. Besl and N. D. McKay, "A method for registration of 3-D shapes," *IEEE Transactions on Pattern Analysis and Machine Intelligence*, vol. 14, no. 2, pp. 239-256, 1992.

[9] J. Goldberger, "Registration of multiple point sets using the EM algorithm," *IEEE International Conference on Computer Vision*, vol. 2, pp. 730-736, 1999.

[10] A. P. Dempster, N. M. Laird, and D. B. Rubin, "Maximum likelihood from incomplete data via the EM algorithm," *Journal of the Royal Statistical Society*, vol. 39, no. 1, pp. 1-22, 1977.

[11] H. Chui and A. Rangarajan, "A new point matching algorithm for non-rigid registrantion," *Computer Vision and Image Understanding*, vol. 89, no. 2-3, pp. 114-141, 2003.

[12] W. Lian, L. Zhang, and M. H. Yang, "An efficient globally optimal algorithm for asymmetric point matching," *IEEE Transactions on Pattern Analysis and Machine Intelligence*, vol. 39, no. 7, pp. 1281-1293, 2017.

[13] B. Jian and B. C. Vemuri, "Robust point set registration using gaussian mixture models," *IEEE Transactions on Pattern Analysis and Machine Intelligence*, vol. 33, no. 8, pp. 1633-1645, 2011.

[14] T. Long, W. Jiao, G. He, and W. Wang, "Automatic line segment registration using gaussian mixture model and expectation-maximization algorithm," *IEEE Journal of Selected Topics in Applied Earth Observations and Remote Sensing*, vol. 7, no. 5, pp. 1688-1699, 2014.

[15] Y. Zhou, S. Xu, C. Jin, and Z. Guo, "Multiple point sets registration based on expectation maximization algorithm," *Computers & Electrical Engineering*, vol. 70, pp. 1-11, 2018.

[16] J. Ma, W. Qiu, J. Zhao, Y. Ma, A. L. Yuille, and Z. Tu, "Robust L_2E estimation of transformation for non-rigid registration," *IEEE Transactions on Signal Processing*, vol. 63, no. 5, pp. 1115-1129, 2015.

[17] J. Ma, J. Zhao, J. Jiang, H. Zhou, and X. Guo, "Locality preserving matching," *International Journal of Computer Vision*, vol. 127, no. 5, pp. 512-531, 2019.

[18] W. Lian and L. Zhang, "Rotaion invariant non-rigid shape matching in cluttered scenes," *European Confernce on Computer Vision*, 2010, pp. 506-518.

[19] W. Lian, L. Zhang, and D. Zhang, "Rotation-invariant nonrigid point set matching in cluttered scenes," *IEEE Transactions on Image Processing*, vol. 21, no. 5, pp. 2786-2797, 2012.

[20] G. Wang, Q. Zhou, and Y. Chen, "Robust non-rigid point set registration using spatially constrained gaussian fields," *IEEE Transactions on Image Processing*, vol. 26, no.4, pp. 1759-1769, 2017.

[21] J. Ma, J. Zhao, and A. L. Yuille, "Non-rigid point set registration by preserving global and local structures," *IEEE Transactions on Image Processing*, vol. 25, no. 1, pp. 53-64, 2016.

[22] A. Myronenko and X. Song, "Point set registration: coherent point drift," *IEEE Transactions on Pattern Analysis and Machine Intelligence*, vol. 32, no. 12, pp. 2262-2275, 2010.

[23] J. Ma, J. Zhao, J. Jiang, and H. Zhong, "Non-rigid point set registration with robust transformation estimation under manifold regularization," *AAAI Conference on Artificial Intelligence*, 2017, pp. 4218-4224.

[24] J. Ma, J. Wu, J. Zhao, J. Jiang, H. Zhou, and Q. Z. Sheng, "Nonrigid point set registration with robust transformation learning under manifold regularization," *IEEE Transactions on Neural Networks and Learning Systems*, DOI:10.1109/TNNLS.2018.2872528, 2019.

[25] H. Zhu, B. Guo, K. Zou, Y. Li, K. V. Yuen, L. Mihaylova, and H. Leung, "A review of point set registration: from pairwise registration to groupwise registration," *Sensors*, vol. 19, no. 5, DOI:10.3390/s19051191, 2019.

[26] A. Rasoulian, R. Rohling, and P. Abolmaesumi, "Group-wise registration of point sets for statistical shape models," *IEEE Transactions on Medical Imaging*, vol. 31, no. 11, pp. 2025-2034, 2012.

[27] G. D. Evangelidis, D. Kounades-Bastian, R. Horaud, E. Z. Psarakis, "A generative model for the joint registration of multiple point sets," *European Conference on Computer Vision*, 2014, pp. 109-122.

[28] G. D. Evangelidis, R. Horaud, "Joint alignment of multiple point sets with batch and incremental expectation-maximization," *IEEE Transactions on Pattern Analysis and Machine Intelligence*, vol. 40, no. 6, pp. 1397-1410, 2018.

[29] L. Torresani, A. Hertzmann, and C. Bregler, "Nonrigid structure-from-motion: estimating shape and motion with hierarchical priors," *IEEE Transactions on Pattern Analysis and Machine Intelligence*, vol. 30, no. 5, pp. 878-892, 2008.

[30] W. Lian, "A path-following algorithm for robust point matching," *IEEE Signal Processing Letters*, vol. 23, no. 1, pp. 89-93, 2015.